Cytokine Profiling in Low- and High-Density Small Extracellular Vesicles from Epidermoid Carcinoma Cells

Joseph P. Flemming[1,4], Brianna L. Hill[1,4], Lauren Anderson-Pullinger[2], Larry A. Harshyne[2] and Mỹ G. Mahoney[1,3]

Exosomes or small extracellular vesicles (sEVs) are membrane-bound nanoparticles that carry various macromolecules and act as autocrine and paracrine signaling messengers. In this study, sEVs from epidermoid carcinoma cells influenced by membrane presentation of the glycoprotein desmoglein 2 and its palmitoylation state were investigated. In this study, sEVs were isolated by sequential ultracentrifugation followed by iodixanol density gradient separation. They were then subjected to multiplex profiling of cytokines associated with the surface of intact sEVs. The results revealed a previously undescribed active sorting of cytokines onto the surface of low-density and high-density sEV subpopulations. Specifically, an altered surface presentation of desmoglein 2 decreased FGF-2 and VEGF in low-density sEVs. In addition, in response to desmoglein 2, IL-8 and RANTES were increased in low-density sEVs but only slightly decreased in high-density sEVs. Finally, IL-6 and G-CSF were increased dramatically in high-density sEVs. This comprehensive analysis of the cytokine production profile by squamous cell carcinoma–derived sEVs highlights their contribution to immune evasion, pro-oncogenic and proangiogenic activity, and the potential to identify diagnostic disease biomarkers.

JID Innovations (2021);**1:**100053 doi:10.1016/j.xjidi.2021.100053

INTRODUCTION

Exosomes are membrane-bound small extracellular vesicles (sEVs) that are secreted by virtually all cell types, that are involved in cell–cell communication, and that play critical roles in health and disease (Abels and Breakefield, 2016; Margolis and Sadovsky, 2019; Roefs et al., 2020). sEVs contain RNA, DNA, proteins, and lipid cargo. Extracellular vesicle (EV) profiling has become even more complex owing to recent evidence of sEV subpopulations, which differ in density and content, including cytokines (Crescitelli et al., 2020; Lázaro-Ibáñez et al., 2019). Cytokines are small molecular weight (~5–20 kDa) signaling proteins secreted by a large variety of cells in response to cellular stresses. They serve a myriad of biological functions, particularly in intercellular communication. In cancer, cytokines can promote tumor cell growth, migration, and metastasis, or as immunoregulators, they can create a microenvironment favorable for tumor growth by stimulating the infiltration of the immunosuppressive myeloid-derived suppressor cells (Taki et al., 2018; Umansky et al., 2016). Recent studies suggest that these cytokines may, in fact, associate with the surface of sEVs by binding to surface proteoglycans, which is essential for sEV–cell interactions (Fitzgerald et al., 2018; Lima et al., 2021). However, it is not known whether these cytokines are differentially associated with subpopulations of sEVs.

We recently showed that the membrane protein desmoglein 2 (Dsg2) modulates sEV biogenesis through the endocytic pathway (Flemming et al., 2020; Overmiller et al., 2017). Dsg2 also activates mitogenic signaling pathways critical for cell growth and survival and promotes cell proliferation and migration (Brennan et al., 2007; Brennan-Crispi et al., 2019, 2015; Overmiller et al., 2016). Furthermore, Dsg2 is highly expressed in many malignancies, including the two most common forms of skin cancers, basal cell carcinoma and squamous cell carcinoma (SCC), and ectopic expression enhances tumor development in mice (Brennan and Mahoney, 2009; Brennan et al., 2007; Brennan-Crispi et al., 2019; Overmiller et al., 2017, 2016). Relevant to this report, we have shown that expression of Dsg2 alters the sEV-associated cytokine secretome of SCC cell lines in vitro, which plays a role in the enhancement of tumorigenesis in a mouse model (Flemming et al., 2020). Although our previous findings helped to elucidate the mechanism by which Dsg2 enhances tumor growth, those findings did not take into account the differential cargo loading between high-density sEVs (HD-sEVs) and low-density sEVs (LD-sEVs). In this study, to distinguish different populations of sEVs; conditioned medium was subjected to ultracentrifugation followed by bottom loading and iodixanol density gradient separation.

[1]*Department of Dermatology & Cutaneous Biology, Thomas Jefferson University, Philadelphia, Pennsylvania, USA;* [2]*Department of Medical Oncology, Thomas Jefferson University, Philadelphia, Pennsylvania, USA; and* [3]*Department of Otolaryngology, Thomas Jefferson University, Philadelphia, Pennsylvania, USA*

[4]*These authors contributed equally to this work.*

Correspondence: Mỹ G. Mahoney, Department of Dermatology & Cutaneous Biology, Thomas Jefferson University, 233 South 10th Street, Suite 428 BLSB, Philadelphia, Pennsylvania 19107, USA. E-mail: My.Mahoney@jefferson.edu

Abbreviations: Dsg2, desmoglein 2; ED, extracellular domain; EV, extracellular vesicle; HD-sEV, high-density small extracellular vesicle; LD-sEV, low-density small extracellular vesicle; SCC, squamous cell carcinoma; sEV, small extracellular vesicle

Received 10 May 2021; revised 21 July 2021; accepted 23 July 2021; accepted manuscript published online XXX; corrected proof published online XXX

Cite this article as: JID Innovations 2021;1:100053

SCC A431 cell lines expressing the constructs of the monomeric-enhanced GFP, Dsg2 fused to GFP (Dsg2/GFP) and unpalmitoylated Dsg2 (Dsg2cacs/GFP), were employed as previously described in detail (Flemming et al., 2020; Roberts et al., 2016). These results shed light on the differential cargo loading between HD-sEVs and LD-sEVs as well as the differences in the membrane-associated cytokine levels in response to the expression of either Dsg2/GFP or Dsg2cacs/GFP. These findings aim to increase the rigor of sEV research and highlight the complex nature of sEV subpopulations with their unique cargo profiles.

RESULTS

Characterization of sEVs by sequential ultracentrifugation and density separation

To explore the effects of Dsg2 and unpalmitoylated Dsg2cacs on EV biogenesis, western blots of each cell line and fraction were performed as described above (Figure 1a). Palmitoylation is a covalent attachment of palmitate, a 16-carbon fatty acid, to cysteine residue. We previously showed that palmitoylation is required for Dsg2 to assemble into desmosomes and for Dsg2 to modulate sEV biogenesis (Flemming et al., 2020; Roberts et al., 2016). In this study, blotting for the tetraspanin marker CD63 (~30–90 kDa) shows where along the density gradient sEVs have localized. Of note, there was a strong CD63 signal in the A431-GFP panel for CD63 mainly in fractions 4 and 5, which represents the 5%/30% interface of the density gradient and is the canonical location of sEVs (Konoshenko et al., 2018). We have named this population of vesicles LD-sEVs. In response to Dsg2/GFP as well as Dsg2cacs/GFP expression, there is a greater CD63 signal present in these same fractions. Interestingly, there is a notable subpopulation of vesicles in fractions 8 and 9 in the A431Dsg2cacs/GFP panel, as indicated by a right shift in the

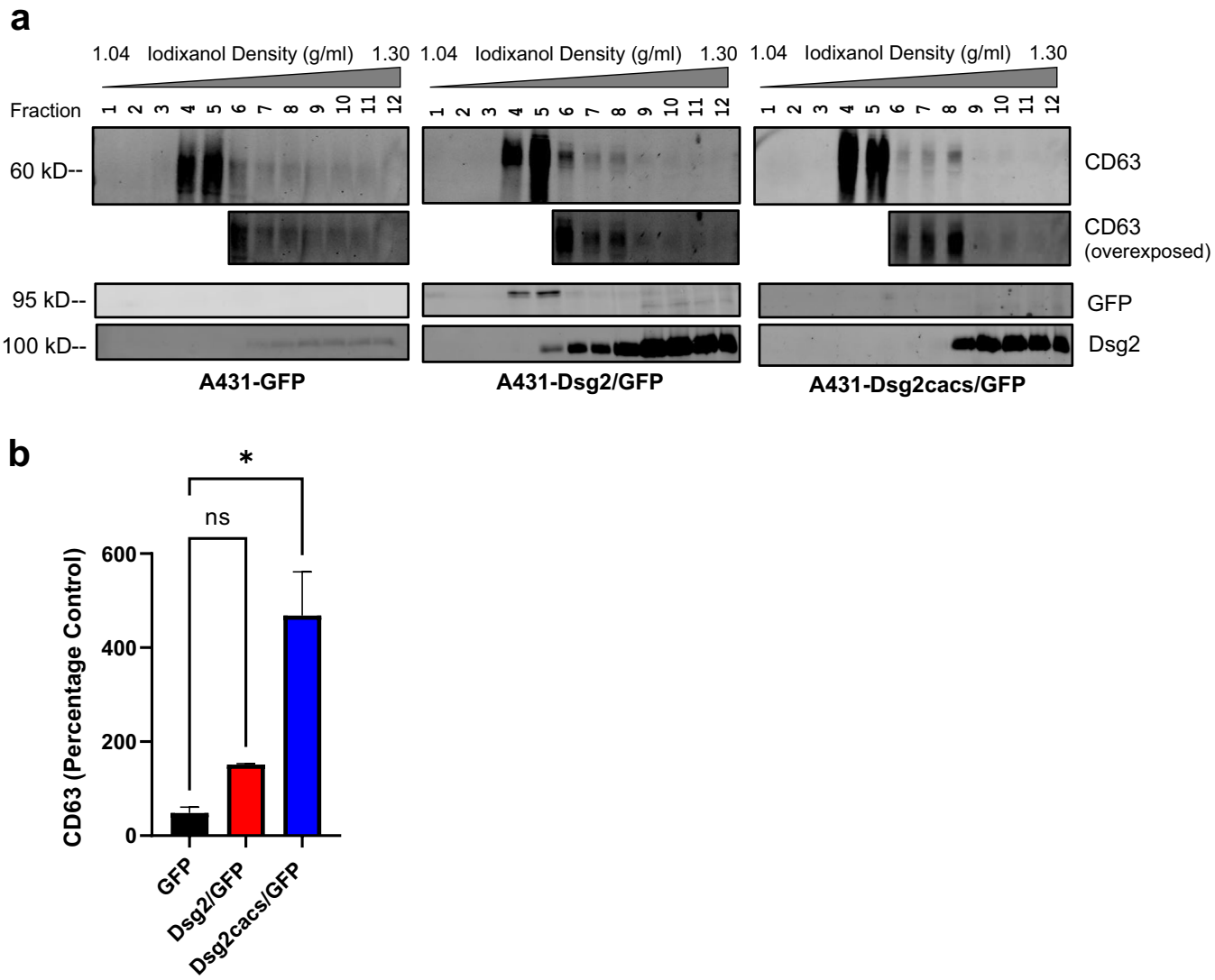

Figure 1. Characterization of sEVs by sequential ultracentrifugation and density gradient separation. (**a**) Conditioned medium was collected from A431 SCC cells stably expressing GFP, Dsg2/GFP, or Dsg2cacs/GFP as a palmitoylation-deficient protein. sEVs were isolated by sequential ultracentrifugation and were further separated over an iodixanol density gradient. Fractions were collected, and proteins were resolved by SDS-PAGE and were immunoblotted with antibodies against Dsg2 (antibody 6D8 against the extracellular domain of Dsg2), GFP, and the tetraspanin marker CD63 (~30–90 kDa). (**b**) Densitometry was performed on fractions 8 and 9 of cells stably expressing GFP, Dsg2/GFP, and Dsg2cacs/GFP to quantitate changes in high-density CD63 levels ($*P < 0.05$). Dsg2, desmoglein 2; ns, not significant; SCC, squamous cell carcinoma; sEV, small extracellular vesicle.

CD63 signal. We have termed this population of vesicles HD-sEVs. Differences in CD63 expression levels are easily appreciated in the overexposed inset found in the second row of Figure 1a. These insets represent the same western blots as their corresponding panels. Quantification of each cell line's high-density fraction was carried out on the basis of the CD63 signal (Figure 1b).

We and others have shown that Dsg2 is cleaved into two major fragments: an ~95 kDa extracellular domain (ED) (Dsg2 ED) and an ~65 kDa C-terminal fragment (Dsg2 C-terminal fragment) (Kolegraff et al., 2011; Overmiller et al., 2017). To further show the difference in the cargo loading between these fractions, immunoblotting for GFP and Dsg2 was performed. As expected, no GFP-linked Dsg2 was detected in A431-GFP cells expressing GFP alone, whereas in Dsg2/GFP cells, a strong signal for the Dsg2 C-terminal fragment linked to GFP (~95 kDa) was observed in the low-density fraction (Figure 1a). Interestingly, no signal was detected for GFP-linked Dsg2 C-terminal fragment in the sEVs from A431-Dsg2cacs/GFP–expressing cells, suggesting either rapid degradation or levels below the limit of detection owing to the loss of palmitoylation. Dsg2 ED was detected at low levels in sEVs from A431-GFP cells owing to their endogenous levels of Dsg2, and forced expression of Dsg2/GFP increased the level of Dsg2 ED in fractions 5–12. In response to Dsg2cacs, Dsg2 ED was only detected in the HD-sEVs and in the protein aggregate fractions. In summary, these results show differential sorting occurring in SCC-derived sEVs modulated by membrane protein presentation.

Comparison of sEV surface-associated cytokines in SCC cells

The presence of cytokines, chemokines, and GFs could affect the signaling potential and pathogenicity of sEVs. In this study, we performed profiling of cytokines associated with the surface of intact sEVs using a 41-plex Luminex assay. The results showed high levels of RANTES, GROα, PDGF-AB/BB, VEGF, G-CSF, IL-8, MDC, IL-1α, IL-1RA, and FGF-2 detected on the surface of A431 sEVs. These observations are illustrated in three ways: a quantitated bar graph, heatmap, and table with numerical values that each represent the average cytokine level of each fraction per cell line (Figure 2a and b and Table 1). Distinct cytokine distributions were also observed in the different density fractions as well as in response to Dsg2 and unpalmitoylated Dsg2cacs. We recently showed that the proinflammatory cytokines IL-6 and IL-8 are upregulated in response to Dsg2. In this study, Dsg2 increased the level of IL-8 and RANTES on LD-sEVs but slightly decreased the level of IL-8 and RANTES on HD-sEVs. Dsg2 expression also resulted in a modest increase of IL-6 and G-CSF in LD-sEVs, with a more substantial increase in the HD-sEV fraction. To identify other cytokines that follow the distribution patterns of IL-6 and IL-8, Pavlidis Template Matching was employed (Figure 2b). Using IL-8 as the template, three cytokines—GROα, IL-1α, and RANTES—were identified, whereas Pavlidis Template Matching using IL-6 identified IL-15, G-CSF, GM-CSF, and PDGF-AB/BB ($R > 0.9$). These results indicate a distinct loading mechanism, mediated by Dsg2 expression in which certain cytokines were preferentially loaded into different subpopulations of sEVs. Cytokine profiling of different density sEVs revealed differential responses to Dsg2 and palmitoylation-disrupted Dsg2cacs, and this disruption of membrane presentation with Dsg2cacs resulted in the reduction of most cytokines associated with both LD-sEVs and HD-sEVs (Figure 2c). In addition to these patterns, we also observed that in response to Dsg2, FGF-2 and VEGF were reduced on LD-sEVs, and the level of FGF-2 remained unchanged on HD-sEVs (Figure 2c). These results indicate active sorting of cytokines onto the surface of sEVs in SCC cells and that their sorting may be dependent on plasma membrane surface proteins and their palmitoylation state.

DISCUSSION

There is a growing body of evidence speaking to the fact that sEVs are remarkably stable and resistant to disruption (Kumeda et al., 2017; Wu et al., 2021). Because sEVs are found in all bodily fluids and are generated with the likely intention of protecting cargo from degradation, it is crucial that they are able to withstand the sheer force experienced while moving through the circulatory system (Boukouris and Mathivanan, 2015; Sanz-Rubio et al., 2018). In fact, this very property is a driving force behind their development as drug delivery systems (Mendt et al., 2018). When considering this knowledge and our own experience with attempts to disrupt sEV membrane integrity, we have concluded that our cytokine results represent surface-associated molecules. We are aware that Luminex's manufacturer protocol does not specifically state whether a given cytokine is surface bound or encapsulated. However, it is a safe assumption that without the addition of detergents, any detected molecules are outside of sEVs. In future experiments, we plan to expand on these results by treating sEVs with detergents to disrupt their membranes and compare this with samples without detergent. This experiment will allow us to definitively state which cytokines are luminal and which are surface bound.

In this study, we have built on our previous findings that IL-8 is found on the surface of LD-sEVs (Flemming et al., 2020) by expanding the analysis to include all density gradient fractions, and the results reveal, to our knowledge, previously unknown information regarding the nature of sEV cargo loading. This study stresses the importance of different isolation methods and their impacts on downstream results of sEV analysis. Specifically, our previous study did not find IL-6 to be associated with sEVs (Flemming et al., 2020). However, this was likely due to our analysis being restricted to the interface of fractions 4 and 5 of the sEV density gradient. By expanding our analysis to include HD-sEVs, we can now conclude that IL-6 is associated with a different sEV subpopulation from IL-8. Cytokines, which are associated with sEVs, may be afforded protection against proteolytic degradation, and they may enhance localized concentration when activating cell surface receptors (Varga et al., 2020). However, the mechanism by which these factors are loaded onto or into vesicles is not well-understood. A critical question remains whether these sEV subpopulations with specific surface-associated cytokines on receptor-mediated internalization

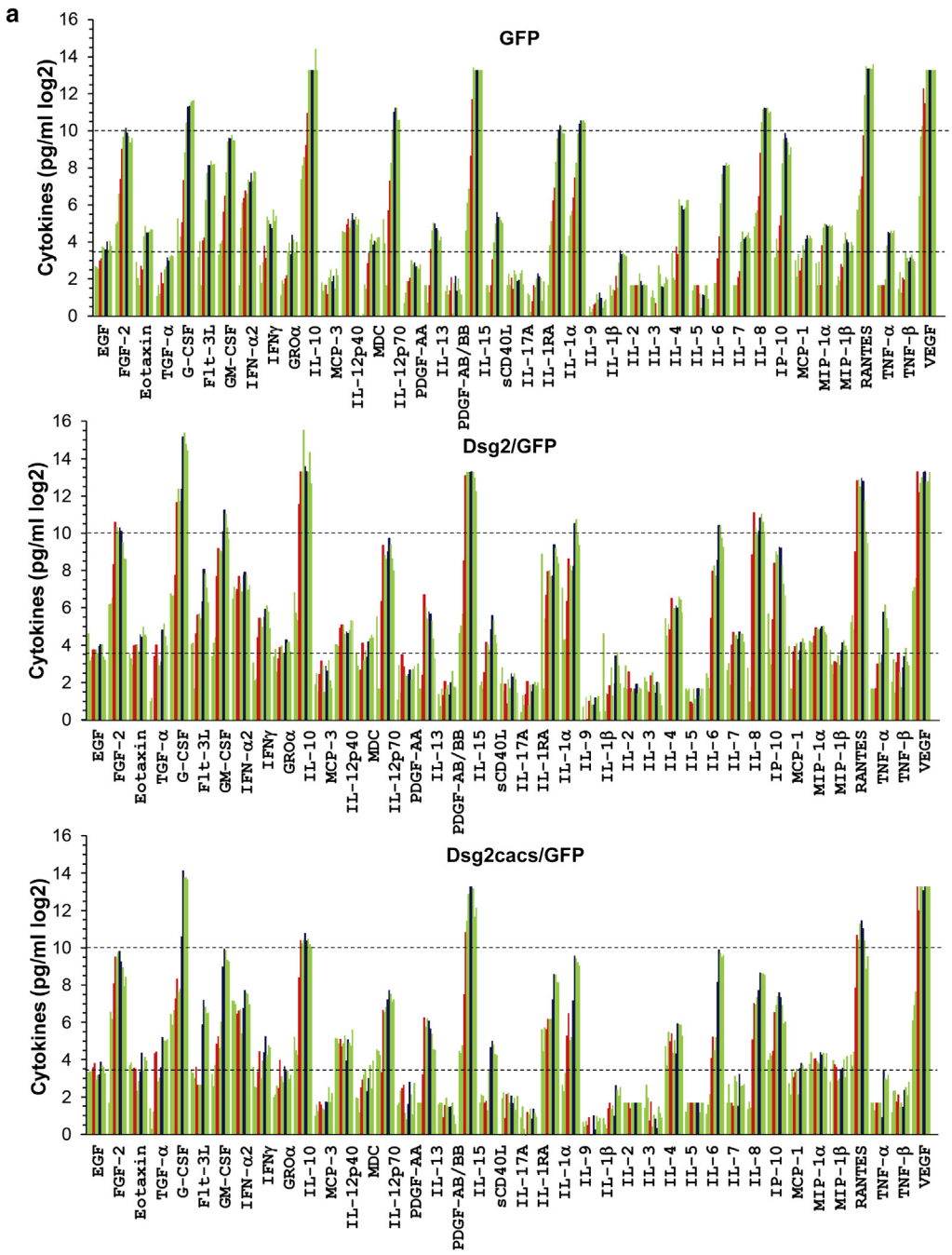

Figure 2. Comparison of sEV surface–associated cytokines in SCC cells. Cytokine profiles of density gradient fractions were characterized through Luminex multiplex analysis, and values in each section represent the average (n = 3) of each fraction, cytokine, and cell line. (**a**) Values from the multiplex analysis also found in Table 1 were plotted and represented as bar graphs for each fraction, cytokine, and cell line for ease of viewing. The red bars indicate LD-sEV fractions, the dark blue bars represent HD-sEVs, and the light green bars represent all other fractions. Note that the dotted lines represent the accurate range of the cytokine array (35–10,000 pg/ml). (**b**) Heatmap showing the unsupervised hierarchical clustering of the cytokines, generated with MultiExperiment Viewer (version 4.9.0). A431-GFP (black), A431-Dsg2/GFP (aquamarine), or A431-Dsg2cacs/GFP (orange) and A431 sEV after UC. Blue corresponds with lower levels of cytokines, and red corresponds with higher levels. Pavlidis Template Matching was performed using IL-8 or IL-6 as the template ($R > 0.9$), and matched genes for each template are shown on the right (IL-8, purple; IL-6, green). (**c**) Representative cytokine (FGF-2, VEGF, IL-8, RANTES, IL-6, and G-CSF) levels measured by multiplex analysis of fractions from density gradient separation—A431-GFP (blue), A431-Dsg2/GFP (red), and A431-Dsg2cacs/GFP (green). Low-density fractions 4 and 5 and high-density fractions 8 and 9 are demarcated. Values from lanes 1–3 and lanes 10–12 are combined. Statistical significance for cytokine levels comparing A431-Dsg2/GFP and A431-Dsg2cacs/GFP with the control (A431-GFP) was determined by ANOVA using Dunnett's post-test. $*P \leq 0.05$, $**P \leq 0.01$, and $***P \leq 0.001$. Dsg2, desmoglein 2; HD-sEV, high-density small extracellular vesicle; LD-sEV, low-density small extracellular vesicle; ns, nonsignificant; SCC, squamous cell carcinoma; sEV, small extracellular vesicle; UC, ultracentrifugation.

would deliver a uniquely packaged content. Obviously, additional sEV studies are warranted, particularly because they may serve not only as biomarkers of diseases but also as cell signaling mechanisms regulating disease processes, thus allowing their possible targeting for therapeutic purposes.

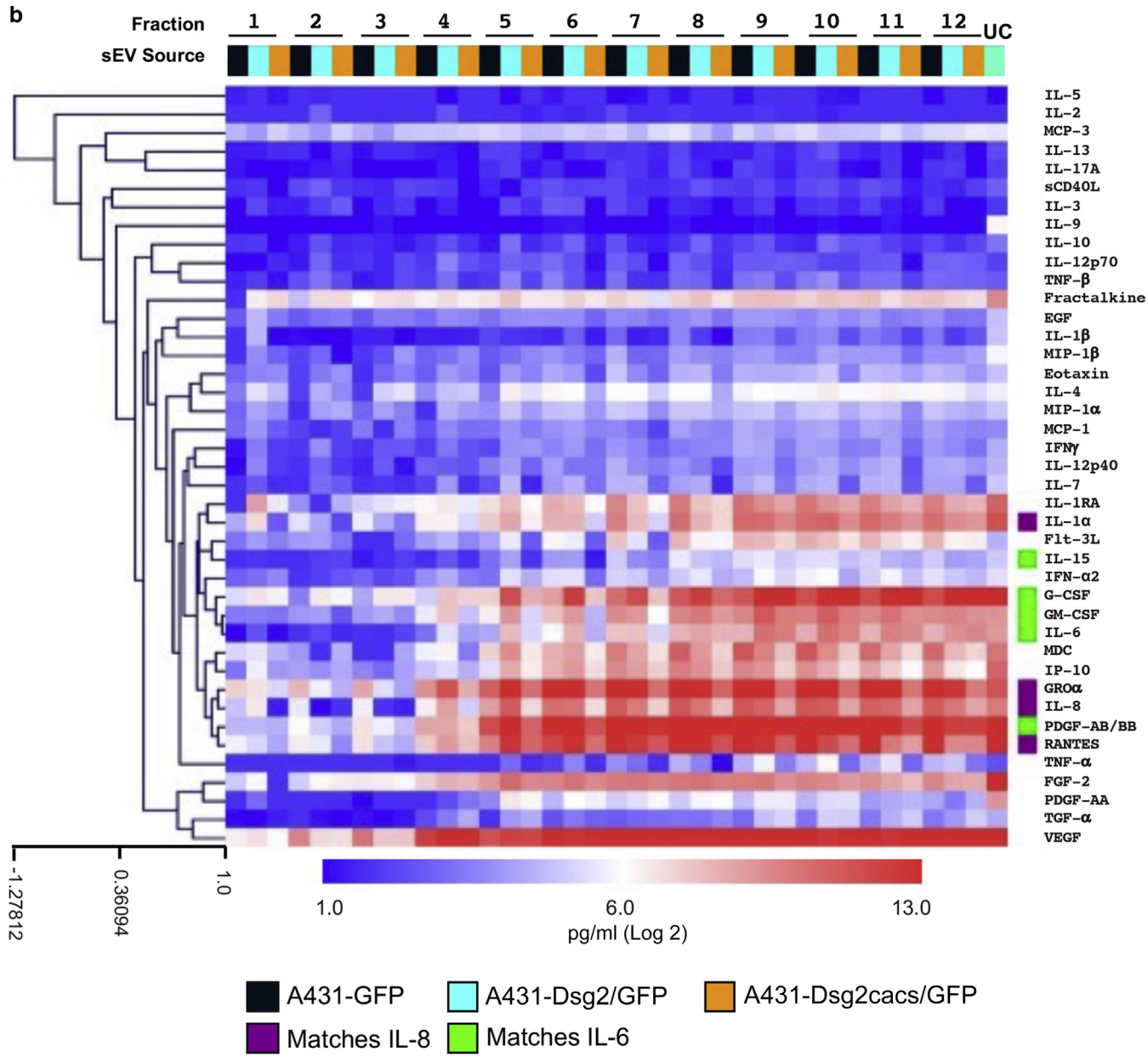

Figure 2. Continued.

MATERIALS AND METHODS

Antibodies

The following antibodies were used for western blotting: 6D8 (Dsg2; 1:100), GFP (1:1,000; Cell Signaling Technologies, Danvers, MA), CD63 (1:1,000; Invitrogen, Carlsbad, CA), goat anti-rabbit or -mouse Odyssey 800 (1:15,000) and 680 (1:20,000, Santa Cruz Biotechnology, Santa Cruz, CA, LI-COR Biosciences, Lincoln, NE).

Cell culture

Generation of GFP, Dsg2/GFP, and mutant Dsg2cacs/GFP (two-point mutations were generated using the QuikChange site–directed mutagenesis kit) cDNA as well as A431-GFP, A431-Dsg2/GFP, and A431-Dsg2cacs/GFP cell lines were previously described in detail (Flemming et al., 2020; Roberts et al., 2016). Briefly, cells (3×10^6) were plated onto 20 (100 mm) culture dishes in a complete growth medium overnight. The cells were then cultivated in a serum-free medium for 48 hours, and the conditioned medium was then collected for EV purification.

Western blotting analysis

For Western blotting, a modified version of the sample preparation protocol, which was previously described in detail, was utilized (Brennan-Crispi et al., 2015; Flemming et al., 2020). Owing to the nature of sEV samples, equal loading was performed in a volume-dependent manner. Briefly, 40 µl of each density gradient fraction was collected, and 10 µl of Laemmli was added to each gradient sample, either with β-mercaptoethanol (for Dsg2 and GFP) or without β-mercaptoethanol (for CD63) as a reducing reagent. After 10 minutes of boiling at 95 °C, 40 µl of each sample was resolved over SDS-PAGE (Bio-Rad Laboratories, Hercules, CA). Infrared bands were visualized and quantitated by the LI-COR Odyssey imaging system (LI-COR Biosciences).

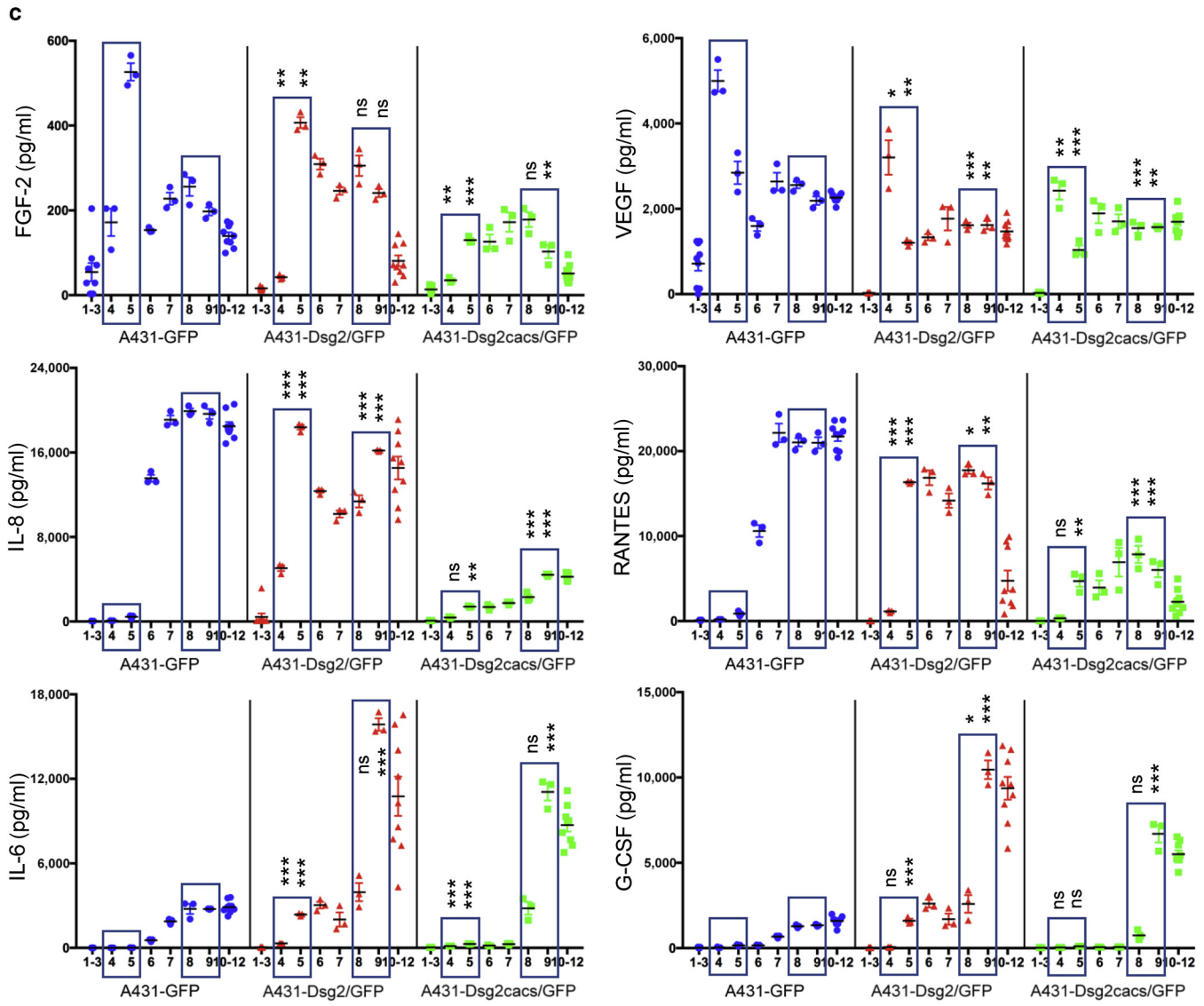

Figure 2. Continued.

EV purification

EV purification was performed using sequential ultracentrifugation protocol: 300*g* (10 minutes), 16,000*g* (30 minutes), and 120,000*g* (70 minutes; Ti45 rotor) (Overmiller et al., 2017). For iodixanol purification, the 120,000*g* pellet containing crude sEVs was suspended in a 40% iodixanol solution and transferred to the bottom of a step gradient composed of 40%/30%/5% iodixanol in 13.2 ml tubes (#331372, polycarbonate tubes, Beckman Coulter, Brea, CA). Samples were centrifuged at 120,000*g* (Sorvall TH 641) for 16 hours overnight at 4 °C, and 1 ml fractions were collected from the top for analysis.

Cytokine luminex analysis

Cytokines were identified by MILLIPLEX MAP Human Cytokine/Chemokine Magnetic Bead Panels according to the manufacturer's instructions. Samples were analyzed in triplicate using MILLIPLEX MAP Human Cytokine/Chemokine Magnetic Bead Panel I kit (HCYTOMAG60K, MilliporeSigma, Burlington, MA) and were run on a FlexMAP 3D (Luminex, Austin, TX). Standard curves were generated for each cytokine, and median fluorescent intensities were transformed into concentrations by five-point, nonlinear regressions.

Heatmap generation and pavlidis template matching

A heatmap was generated using $\log_2$ transformed values in MultiExperiment Viewer (version 4.9.0). Hierarchical clustering was performed using the Pearson correlation coefficient as the distance metric and average linkage in MultiExperiment Viewer. Pavlidis Template Matching was performed in MultiExperiment Viewer using an R threshold > 0.9 using either IL-8 or IL-6 as the template.

Data availability statement

No datasets were generated or analyzed during this study.

ORCIDs
Joseph P. Flemming: http://orcid/org/0000-0002-9947-1456
Brianna L. Hill: http://orcid/org/0000-0002-9973-5765
Lauren Anderson-Pullinger: http://orcid/org/0000-0001-5365-7944
Larry A. Harshyne: http://orcid/org/0000-0002-8699-3028
Mỹ G. Mahoney: http://orcid/org/0000-0003-0203-9171

Table 1. Comparison of sEV Surface Cytokines, Chemokines, and GFs following Density Gradient Separation

	A431-GFP											
	5% Iodixanol				30% Iodixanol				40% Iodixanol			
	1	2	3	4	5	6	7	8	9	10	11	12
EGF	6.4	6.4	5.9	8.0	8.7	13.6	13.0	12.1	16.3	12.0	16.7	14.0
FGF-2	31.4	34.3	98.0	171.8	526.6	818.2	1,058.6	1,140.7	965.6	843.6	660.9	788.9
Eotaxin	7.6	4.2	3.2	6.6	5.6	19.8	29.4	23.0	23.0	23.7	26.0	25.5
TGF-α	2.1	3.2	2.3	5.1	3.4	5.7	6.4	9.0	8.0	9.3	9.9	9.4
G-CSF	38.8	10.6	19.8	33.7	161.2	460.6	1,397.8	2,529.3	2,638.1	2,995.8	3,190.9	3,263.7
Flt-3L	9.2	16.4	3.2	17.0	18.9	77.8	212.1	285.3	285.2	334.5	291.2	294.5
GM-CSF	9.9	15.3	16.9	49.6	90.9	220.2	683.5	796.4	776.1	880.3	723.0	711.3
Fractalkine	3.2	27.3	70.4	82.9	109.0	99.4	165.0	150.7	210.0	156.2	226.4	222.6
IFN-α2	6.8	3.4	7.5	14.0	8.9	42.0	36.3	31.5	26.7	54.0	35.0	42.6
IFN-γ	2.2	3.8	3.4	4.0	4.6	11.3	15.5	10.1	20.8	17.7	11.0	16.0
GROα	166.3	280.3	386.3	604.4	2,022.5	10,000.0	10,000.0	10,000.0	10,000.0	10,000.0	22,227.4	10,000.0
IL-10	3.5	2.6	3.2	3.2	2.3	4.2	5.7	3.6	4.6	2.8	5.9	4.6
MCP3	24.0	23.5	22.8	30.8	38.3	27.2	36.1	47.2	37.0	41.8	30.2	37.8
IL-12p40	1.1	3.3	2.8	7.2	10.7	17.4	21.9	14.6	16.6	16.2	18.9	19.2
MDC	37.5	15.2	3.2	52.3	158.9	308.9	1,001.9	2,093.5	2,460.1	2,423.9	1,544.8	1,558.4
IL-12p70	1.6	2.4	3.7	3.7	4.2	8.1	6.9	7.3	6.5	6.5	5.9	7.0
PDGF-AA	3.2	3.2	1.7	3.2	12.2	24.5	33.0	31.8	26.6	24.6	17.0	19.4
IL-13	2.5	3.2	2.2	2.6	4.3	1.1	3.5	4.6	2.6	4.1	2.7	2.2
PDGF-AB/BB	24.7	69.8	117.3	405.3	3,378.4	10,871.0	10,000.0	10,000.0	10,000.0	10,000.0	10,000.0	10,000.0
IL-15	3.2	3.2	2.4	3.2	8.4	15.8	32.1	48.8	41.2	40.8	36.0	32.3
sCD40L	3.2	4.9	3.2	4.2	2.7	5.5	4.7	3.7	3.9	4.9	5.6	3.3
IL-17A	2.4	2.2	1.2	1.7	3.2	3.0	4.1	5.0	4.4	4.2	1.8	3.6
IL-1RA	3.2	14.2	35.2	76.5	121.1	323.0	776.9	1,071.6	1,268.9	1,217.4	935.5	931.4
IL-1α	20.3	43.3	51.1	84.2	178.8	308.2	933.5	1,352.6	1,507.5	1,485.8	1,513.7	1,401.7
IL-9	1.4	1.2	1.3	1.5	1.6	2.3	1.9	2.4	2.0	1.4	1.8	1.9
IL-1β	3.2	2.1	2.7	2.6	4.5	2.9	7.4	11.8	10.1	10.6	10.0	9.5
IL-2	3.2	3.2	3.2	3.2	3.2	3.2	4.9	3.7	3.2	3.3	3.2	3.2
IL-3	2.1	2.6	2.0	1.6	1.0	6.7	4.9	3.1	3.0	3.4	4.3	3.9
IL-4	10.5	4.2	3.8	13.5	10.2	78.3	62.4	62.7	54.4	57.8	75.4	76.9
IL-5	2.6	3.2	3.2	3.2	3.2	2.3	1.4	2.2	2.2	3.2	3.2	1.9
IL-6	1.1	3.5	3.5	8.7	19.9	67.9	203.0	281.6	281.3	312.7	278.8	288.8
IL-7	3.2	3.2	3.2	4.3	5.4	16.0	23.6	18.0	19.1	20.5	22.9	18.6
IL-8	28.7	48.2	52.2	89.4	446.2	1,409.8	2,300.5	2,461.0	2,410.6	2,432.8	2,001.3	2,141.7
IP-10	9.1	18.3	11.7	29.6	43.1	304.4	744.7	937.8	789.4	658.2	418.9	555.5
MCP-1	8.1	4.3	10.2	5.5	8.9	14.2	12.2	17.8	20.7	18.3	20.1	18.4
MIP-1α	7.3	3.2	7.6	3.2	14.3	27.3	31.9	30.5	28.6	30.3	28.4	29.6
MIP-1β	3.2	4.5	3.8	7.0	6.3	14.9	22.7	17.5	15.7	11.1	16.1	14.3
RANTES	53.4	92.8	115.8	185.4	870.6	3,959.7	11,498.6	10,505.3	10,472.4	10,653.2	10,418.7	12,291.8
TNF-α	3.2	3.2	3.2	3.2	3.2	4.0	13.9	23.4	22.5	24.7	22.6	24.4
TNF-β	2.7	5.2	2.4	4.2	4.0	11.1	8.9	7.9	8.9	10.0	8.5	7.9
VEGF	89.6	830.2	1,225.9	4,998.0	2,845.6	10,000.0	10,000.0	10,000.0	10,000.0	10,000.0	10,000.0	10,000.0
	A431-Dsg2/GFP											
	5% Iodixanol				30% Iodixanol				40% Iodixanol			
	1	2	3	4	5	6	7	8	9	10	11	12
EGF	24.8	8.9	10.4	13.4	13.3	13.5	11.8	15.4	16.3	16.6	10.2	9.3
FGF-2	73.1	74.5	94.3	318.1	1,534.7	1,289.2	1,113.7	1,277.5	1,098.5	727.4	398.9	397.1
Eotaxin	11.8	9.8	7.7	15.7	16.0	16.4	12.7	24.2	21.6	31.6	23.7	22.4
TGF-α	2.0	2.2	0.7	10.4	16.0	9.8	7.5	8.8	27.8	35.3	22.0	16.2
G-CSF	108.2	99.3	103.1	212.8	3,172.7	5,339.8	3,377.7	5,368.6	36,327.0	42,606.7	27,806.0	22,705.0
Flt-3L	16.9	17.4	3.2	24.1	49.2	51.2	43.2	81.4	266.6	228.8	134.9	79.0
GM-CSF	10.7	17.4	21.4	205.9	577.3	546.3	522.3	1,102.4	2,426.2	2,054.5	1,254.9	828.3
Fractalkine	89.8	139.9	112.2	125.5	206.3	160.0	118.0	218.3	238.7	220.3	124.5	151.2
IFN-α2	8.4	4.3	4.6	21.2	42.8	43.0	31.2	45.9	60.2	69.5	55.2	30.3
IFN-γ	10.5	13.9	6.0	9.6	14.5	15.7	12.0	11.7	19.2	17.2	18.0	12.7

(*continued*)

Table 1. Continued

	A431-Dsg2/GFP											
	5% Iodixanol				30% Iodixanol				40% Iodixanol			
	1	2	3	4	5	6	7	8	9	10	11	12
GROα	112.3	53.1	40.9	2,964.1	10,000.0	10,000.0	47,132.4	12,387.1	10,000.0	10,000.0	20,841.3	6,445.9
IL-10	3.7	5.6	2.8	5.3	8.7	7.5	2.8	7.4	6.1	9.0	4.2	3.3
MCP3	16.4	16.1	15.4	29.9	33.5	34.0	24.0	26.9	24.7	27.9	39.9	39.9
IL-12p40	12.1	7.3	6.3	6.3	17.1	9.1	13.2	10.3	18.0	20.7	23.5	21.4
MDC	46.0	3.2	3.2	81.2	654.2	460.6	388.7	519.0	848.1	678.1	400.9	258.6
IL-12p70	2.1	7.6	2.8	11.2	7.2	5.4	5.1	5.5	6.3	4.4	6.5	7.4
PDGF-AA	8.1	3.2	3.2	5.2	103.8	66.2	42.8	56.4	50.3	39.8	20.2	9.8
IL-13	2.6	1.7	3.2	2.4	4.1	3.1	3.7	2.6	3.9	6.1	3.4	3.4
PDGF-AB/BB	25.0	33.4	51.6	364.2	8,603.3	10,000.0	10,000.0	10,000.0	10,000.0	10,000.0	8,115.8	4,923.7
IL-15	3.6	4.2	3.2	5.8	17.6	16.4	13.3	29.2	47.8	41.6	23.4	17.2
sCD40L	3.8	7.0	2.9	3.7	1.8	4.5	3.2	5.6	4.8	5.6	4.5	2.7
IL-17A	1.3	2.5	1.7	2.5	4.1	1.7	3.7	2.9	3.7	4.1	3.5	4.0
IL-1RA	476.9	3.2	43.6	101.0	244.0	255.7	204.7	213.8	661.5	585.9	426.7	335.8
IL-1α	134.8	19.6	20.1	80.5	388.8	307.8	256.3	301.2	1,452.0	1,692.2	983.4	670.9
IL-9	1.6	0.9	2.3	0.8	2.0	2.4	1.8	1.8	2.2	2.2	2.4	1.4
IL-1β	24.7	1.4	2.7	2.5	3.5	7.0	2.5	3.9	10.7	12.3	7.5	3.9
IL-2	3.3	7.5	3.1	5.8	3.2	2.8	3.2	3.2	3.7	2.6	3.3	3.1
IL-3	4.8	4.2	3.0	2.8	5.1	5.9	3.7	2.7	4.0	3.9	2.6	1.7
IL-4	43.2	22.4	35.3	28.3	90.5	63.8	63.1	70.1	63.5	96.6	86.3	54.1
IL-5	3.2	3.0	3.2	1.9	1.8	3.2	2.2	3.2	3.2	2.4	3.2	3.2
IL-6	5.5	4.7	3.2	42.9	246.8	305.3	212.9	383.4	1,350.1	1,318.9	864.3	621.2
IL-7	6.3	8.2	3.7	15.9	25.5	23.0	23.5	20.3	26.1	24.4	24.1	18.3
IL-8	97.7	2.0	3.5	461.4	2,168.5	1,250.8	991.0	1,132.0	1,794.0	2,101.4	1,562.1	1,086.1
IP-10	51.7	13.9	7.8	40.8	337.1	517.1	455.8	625.9	584.3	316.2	155.0	102.3
MCP-1	15.4	3.2	3.2	12.5	15.1	17.0	9.3	13.2	17.6	20.4	17.4	13.5
MIP-1α	18.6	17.5	17.9	22.2	30.3	29.3	28.5	29.5	31.7	32.4	25.8	24.0
MIP-1β	13.4	7.8	5.4	8.6	8.2	10.8	7.6	13.3	17.3	19.3	15.7	13.7
RANTES	37.2	49.0	28.9	505.9	7,100.0	7,458.0	5,812.5	8,025.7	7,022.6	3,405.3	1,087.6	714.3
TNF-α	3.2	3.2	3.2	3.2	7.9	11.7	8.3	11.4	54.1	72.0	43.4	30.4
TNF-β	4.0	9.4	2.7	8.3	11.7	5.8	3.4	7.1	10.4	14.3	8.6	7.5
VEGF	119.8	136.1	195.1	10,000.0	4,626.6	6,665.6	8,214.0	10,000.0	10,000.0	6,641.1	6,990.3	10,000.0
	A431-Dsg2CACS/GFP											
	5% Iodixanol				30% Iodixanol				40% Iodixanol			
	1	2	3	4	5	6	7	8	9	10	11	12
EGF	10.1	10.2	10.3	11.9	13.9	7.6	8.9	9.2	14.7	12.8	12.0	9.5
FGF-2	3.2	94.5	72.9	267.8	731.8	713.7	879.0	900.7	618.4	493.4	241.2	347.4
Eotaxin	13.1	14.4	11.3	11.8	11.4	5.0	7.2	10.3	20.5	10.8	17.8	15.4
TGF-α	2.6	1.2	2.3	20.1	21.3	7.1	8.2	11.9	36.4	32.5	32.0	33.9
G-CSF	86.1	58.4	100.1	154.0	322.1	197.0	223.3	1,545.5	17,979.0	13,827.7	14,006.9	12,947.6
Flt-3L	10.9	9.6	8.0	12.2	6.3	6.3	6.3	58.7	145.7	111.9	89.2	91.1
GM-CSF	9.4	5.9	13.2	28.9	38.0	24.5	64.8	506.0	983.3	943.0	644.5	616.8
Fractalkine	143.4	140.7	125.0	87.3	97.2	103.6	42.2	109.0	210.0	188.9	183.8	124.4
IFN-α2	12.2	5.9	5.6	10.2	21.6	8.0	15.2	20.8	38.1	18.9	27.3	25.3
IFN-γ	4.0	4.3	6.0	5.6	15.8	8.5	6.9	12.3	10.3	10.7	7.7	9.0
GROα	37.6	22.6	18.8	337.3	1,358.5	1,202.0	1,355.8	1,745.0	1,315.7	1,428.1	1,161.5	1,051.0
IL-10	2.0	3.0	2.4	3.3	3.0	2.6	2.5	3.3	3.3	5.8	3.3	4.6
MCP3	35.6	34.8	29.1	34.0	25.7	29.4	38.9	15.2	33.8	29.8	26.9	48.5
IL-12p40	3.9	3.8	2.2	5.6	7.6	9.1	10.5	4.9	8.1	13.1	5.4	15.4
MDC	23.1	22.2	18.8	10.1	100.5	93.0	111.6	148.6	210.6	183.5	137.6	150.0
IL-12p70	3.0	3.2	5.0	5.5	6.3	2.2	1.7	3.1	7.0	4.3	2.1	6.7
PDGF-AA	3.2	3.2	3.2	9.3	76.0	53.8	74.0	67.3	50.1	41.8	23.6	23.1
IL-13	3.1	3.2	3.2	1.9	2.9	3.8	2.8	2.7	2.8	3.2	2.0	1.5
PDGF-AB/BB	22.3	20.2	27.3	179.1	1,815.3	2,774.5	7,549.6	10,000.0	10,000.0	9,216.2	3,242.6	4,530.6
IL-15	3.2	4.3	4.2	3.2	3.4	2.4	10.5	25.4	31.9	27.7	19.7	19.0

(*continued*)

Table 1. Continued

	A431-Dsg2CACS/GFP											
	5% Iodixanol				30% Iodixanol				40% Iodixanol			
	1	2	3	4	5	6	7	8	9	10	11	12
sCD40L	1.0	3.7	4.7	1.8	4.4	4.6	3.2	4.2	3.2	3.8	2.5	4.1
IL-17A	1.8	2.8	1.2	0.9	2.3	2.1	2.6	1.8	2.6	2.2	1.9	0.9
IL-1RA	49.4	21.9	52.9	49.6	73.2	71.7	73.0	149.1	385.8	378.1	283.0	277.8
IL-1α	6.3	4.9	9.8	38.5	90.1	33.1	37.0	144.8	762.6	684.6	590.4	524.6
IL-9	1.6	1.3	1.6	1.4	1.9	0.9	0.8	2.0	1.2	1.9	1.6	1.8
IL-1β	1.8	1.4	1.2	2.6	3.2	2.5	2.9	2.0	6.2	5.2	4.2	5.8
IL-2	3.2	3.2	3.2	3.2	2.6	3.2	3.2	3.2	3.2	3.2	3.2	3.2
IL-3	2.6	6.3	3.8	1.7	3.3	1.3	2.1	1.8	1.2	2.8	2.2	1.8
IL-4	26.2	12.8	44.4	31.6	42.4	20.5	33.1	19.8	61.3	59.9	57.8	38.5
IL-5	2.3	3.2	3.2	3.2	3.2	3.2	3.2	3.2	3.2	2.2	3.2	3.2
IL-6	2.1	3.0	4.4	17.1	37.2	22.3	36.5	284.8	956.4	821.4	716.2	768.9
IL-7	3.2	6.3	3.2	3.2	2.8	8.7	7.0	2.8	9.4	6.0	6.1	6.3
IL-8	2.5	3.3	2.6	33.7	130.0	125.8	161.2	211.6	402.4	394.1	392.7	369.1
IP-10	15.8	20.2	18.5	22.0	92.3	120.2	167.4	192.4	161.9	121.7	60.8	65.9
MCP-1	6.6	4.3	10.9	8.4	10.1	11.3	4.3	11.6	14.1	13.0	10.7	11.6
MIP-1α	13.4	21.2	10.9	16.3	16.8	15.2	13.8	20.8	19.1	20.5	12.2	20.3
MIP-1β	7.1	0.6	15.6	13.3	12.1	7.3	7.9	11.2	11.7	16.2	8.3	18.1
RANTES	19.4	12.6	21.2	232.5	1,631.4	1,385.9	2,472.8	2,794.7	2,090.6	1,333.0	466.8	746.1
TNF-α	3.2	3.2	2.4	3.2	3.2	3.2	3.2	1.9	10.6	7.9	7.7	9.1
TNF-β	2.3	5.0	5.1	3.3	4.4	2.7	3.2	2.8	5.2	5.7	4.3	7.0
VEGF	69.1	121.5	201.1	10,000.0	4,037.9	10,000.0	10,000.0	8,693.1	10,000.0	10,000.0	10,000.0	10,000.0

sEVs were isolated by sequential ultracentrifugation from conditioned medium of SCC A431 cells overexpressing GFP, Dsg2/GFP, or Dsg2CACS/GFP, and the exosome crude pellet was further separated by iodixanol density gradient. sEVs were subjected to multiplex cytokine analysis for surface but not encapsulated cytokines (pg/ml). Levels below 35 pg/ml or above 10,000 pg/ml were considered as below or above the limit of detection, respectively. All values represent averages of three reads for each fraction.

Abbreviations: SCC, squamous cell carcinoma; sEV, small extracellular vesicle.

AUTHOR CONTRIBUTIONS

Conceptualization: MGM; Data Curation: JPF, BLH, LAP, LAH, MGM; Formal Analysis: JPF, BLH, LAP, LAH, MGM; Funding Acquisition: MGM; Investigation: MGM; Methodology: JPF, BLH, LAP, LAH, MGM; Project Administration: MGM; Resources: MGM; Supervision: MGM; Validation: JPF, BLH, LAP, LAH, MGM; Visualization: JPF, BLH, LAP, LAH, MGM; Writing - Original Draft Preparation: JPF, BLH, MGM; Writing - Review and Editing: JPF, BLH, LAH, MGM

ACKNOWLEDGMENTS

We sincerely thank Alyssa Calder, Sydney Gilmore, and Abigail LaCour for critically reading this manuscript. We also thank James K. Wahl III (University of Nebraska-Lincoln) for the A431-GFP, A431-desmoglein 2/GFP, and A431-desmoglein 2cacs/GFP cell lines. This study was supported by grants from the National Institutes of Health National Institute of Arthritis and Musculoskeletal and Skin Diseases R01-AR074314 to MGM and T32-AA007463 (trainee recipient BLH), and the Clinical Cancer Immunology Core is supported by the Sidney Kimmel Cancer Center (Thomas Jefferson University) Support grant 5P30CA056036-20.

CONFLICT OF INTEREST

The authors state no conflict of interest.

REFERENCES

Abels ER, Breakefield XO. Introduction to extracellular vesicles: biogenesis, RNA cargo selection, content, release, and uptake. Cell Mol Neurobiol 2016;36:301–12.

Boukouris S, Mathivanan S. Exosomes in bodily fluids are a highly stable resource of disease biomarkers. Proteomics Clin Appl 2015;9:358–67.

Brennan D, Hu Y, Joubeh S, Choi YW, Whitaker-Menezes D, O'Brien T, et al. Suprabasal Dsg2 expression in transgenic mouse skin confers a hyperproliferative and apoptosis-resistant phenotype to keratinocytes. J Cell Sci 2007;120:758–71.

Brennan D, Mahoney MG. Increased expression of Dsg2 in malignant skin carcinomas: a tissue-microarray based study. Cell Adh Migr 2009;3:148–54.

Brennan-Crispi DM, Hossain C, Sahu J, Brady M, Riobo NA, Mahoney MG. Crosstalk between desmoglein 2 and patched 1 accelerates chemical-induced skin tumorigenesis. Oncotarget 2015;6:8593–605.

Brennan-Crispi DM, Overmiller AM, Tamayo-Orrego L, Marous MR, Sahu J, McGuinn KP, et al. Overexpression of desmoglein 2 in a mouse model of Gorlin syndrome enhances spontaneous basal cell carcinoma formation through STAT3-mediated Gli1 expression. J Invest Dermatol 2019;139:300–7.

Crescitelli R, Lässer C, Jang SC, Cvjetkovic A, Malmhäll C, Karimi N, et al. Subpopulations of extracellular vesicles from human metastatic melanoma tissue identified by quantitative proteomics after optimized isolation. J Extracell Vesicles 2020;9:1722433.

Fitzgerald W, Freeman ML, Lederman MM, Vasilieva E, Romero R, Margolis L. A system of cytokines encapsulated in extracellular vesicles [published correction appears in Sci Rep 2020;10:18935]. Sci Rep 2018;8:8973.

Flemming JP, Hill BL, Haque MW, Raad J, Bonder CS, Harshyne LA, et al. miRNA- and cytokine-associated extracellular vesicles mediate squamous cell carcinomas. J Extracell Vesicles 2020;9:1790159.

Kolegraff K, Nava P, Laur O, Parkos CA, Nusrat A. Characterization of full-length and proteolytic cleavage fragments of desmoglein-2 in native human colon and colonic epithelial cell lines. Cell Adh Migr 2011;5:306–14.

Konoshenko MY, Lekchnov EA, Vlassov AV, Laktionov PP. Isolation of extracellular vesicles: general methodologies and latest trends. BioMed Res Int 2018;2018:8545347.

Kumeda N, Ogawa Y, Akimoto Y, Kawakami H, Tsujimoto M, Yanoshita R. Characterization of membrane integrity and morphological stability of human salivary exosomes. Biol Pharm Bull 2017;40:1183–91.

Lázaro-Ibáñez E, Lässer C, Shelke GV, Crescitelli R, Jang SC, Cvjetkovic A, et al. DNA analysis of low- and high-density fractions defines heterogeneous

subpopulations of small extracellular vesicles based on their DNA cargo and topology. J Extracell Vesicles 2019;8:1656993.

Lima LG, Ham S, Shin H, Chai EPZ, Lek ESH, Lobb RJ, et al. Tumor microenvironmental cytokines bound to cancer exosomes determine uptake by cytokine receptor-expressing cells and biodistribution. Nat Commun 2021;12:3543.

Margolis L, Sadovsky Y. The biology of extracellular vesicles: the known unknowns. PLoS Biol 2019;17:e3000363.

Mendt M, Kamerkar S, Sugimoto H, McAndrews KM, Wu CC, Gagea M, et al. Generation and testing of clinical-grade exosomes for pancreatic cancer. JCI Insight 2018;3:e99263.

Overmiller AM, McGuinn KP, Roberts BJ, Cooper F, Brennan-Crispi DM, Deguchi T, et al. c-Src/Cav1-dependent activation of the EGFR by Dsg2. Oncotarget 2016;7:37536–55.

Overmiller AM, Pierluissi JA, Wermuth PJ, Sauma S, Martinez-Outschoorn U, Tuluc M, et al. Desmoglein 2 modulates extracellular vesicle release from squamous cell carcinoma keratinocytes. FASEB J 2017;31:3412–24.

Roberts BJ, Svoboda RA, Overmiller AM, Lewis JD, Kowalczyk AP, Mahoney MG, et al. Palmitoylation of desmoglein 2 is a regulator of assembly dynamics and protein turnover. J Biol Chem 2016;291:24857–65.

Roefs MT, Sluijter JPG, Vader P. Extracellular vesicle-associated proteins in tissue repair. Trends Cell Biol 2020;30:990–1013.

Sanz-Rubio D, Martin-Burriel I, Gil A, Cubero P, Forner M, Khalyfa A, et al. Stability of circulating exosomal miRNAs in healthy subjects. Sci Rep 2018;8:10306.

Taki M, Abiko K, Baba T, Hamanishi J, Yamaguchi K, Murakami R, et al. Snail promotes ovarian cancer progression by recruiting myeloid-derived suppressor cells via CXCR2 ligand upregulation. Nat Commun 2018;9:1685.

Umansky V, Blattner C, Gebhardt C, Utikal J. The role of myeloid-derived suppressor cells (MDSC) in cancer progression. Vaccines (Basel) 2016;4:36.

Varga Z, Fehér B, Kitka D, Wacha A, Bóta A, Berényi S, et al. Size measurement of extracellular vesicles and synthetic liposomes: the impact of the hydration shell and the protein corona. Colloids Surf B Biointerfaces 2020;192:111053.

Wu JY, Li YJ, Hu XB, Huang S, Xiang DX. Preservation of small extracellular vesicles for functional analysis and therapeutic applications: a comparative evaluation of storage conditions. Drug Deliv 2021;28:162–70.